Progress In Electromagnetics Research C, Vol. 85, 77–89, 2018

Object Locating of Electromagnetic Inclusions in Anisotropic Permeable Background Using MUSIC Algorithm

Faezeh Shirmehenji, Abolghasem Zeidaabadi-Nezhad*, and Zaker Hossein Firouzeh

Abstract—In this paper, a new formulation is proposed to solve an inverse scattering problem for locating isolated inclusions within a homogeneous noise-free and noisy biaxial anisotropic permeable background using MUltiple SIgnal Classification (MUSIC) algorithm. Locations of the dielectric, permeable, lossless and lossy electromagnetic or both dielectric and permeable inclusions with arbitrary ellipsoidal shapes can be restored. The numerical study of different inclusions is illustrated, and accuracy of the method is investigated. The proposed formulation is also investigated for extended inclusions backgrounds.

1. INTRODUCTION

Inverse scattering of electromagnetic waves is used in many applications such as the imaging of weather patterns, military radars, and nondestructive testing (NDT) such as the detection of a crack in a bridge [1–3]. Inverse scattering problems are investigated and solved by qualitative and quantitative methods. The qualitative methods yield shape and locations of the scatterers. The quantitative methods besides of shape and location give electromagnetic properties of scatterers, such as permittivity and permeability [3].

The MUltiple SIgnal Classification (MUSIC) algorithm which is a qualitative method is used only for point inclusions; however, multipath scattering between the inclusions is not taken into account by this algorithm. The transmitter and receiver antennas are in the far field of the inclusions. This algorithm also uses scattering waves to form multi-static response matrix. If the number of transmitter antennas is more than the number of inclusions, the required condition of MUSIC algorithm is provided [4]. This non-iterative algorithm needs less computation time than all of the quantitative methods. So, it can be used as an initial guess for the quantitative methods [5]. Another advantage of this algorithm is that it uses closed-form function for analysis.

In [6, 7] the MUSIC algorithm is employed to detect small two-dimensional cylinders. This approach cannot reconstruct the exact contour of large cylindrical scatterers, but it provides some information of them, such as the number of cylinders and their approximate location. In [8] and [9], this approach is used for imaging of the perfect conductor cracks; however, shape of the inclusions cannot be reconstructed. The MUSIC algorithm is also used to detect an inhomogeneous thin dielectric structure in a two-dimensional homogeneous space in [10] and electromagnetic structure in [11]. Time-Reversal MUSIC (TRM), investigated in [12–14] and [15], is used for multiple scattering among the scatterers, but it is not as simple as MUSIC. TRM imaging of extended targets has been investigated in [15].

In [16, 17] the locations of two and three dimensional ellipsoidal inclusions in free space are found, and the locations of three dimensional cubical inclusions are determined in an anisotropic background in [18] and ellipsoidal inclusions in [19].

Received 19 April 2018, Accepted 21 June 2018, Scheduled 6 July 2018

* Corresponding author: Abolghasem Zeidaabadi-Nezhad (zeidabad@cc.iut.ac.ir).
The authors are with the Department of Electrical and Computer Engineering, Isfahan University of Technology (IUT), Isfahan 84156-83111, Iran.

The macroscopic properties of an anisotropic electromagnetic material can be modeled by a tensor which describes dependency of the material permittivity and permeability on the wave direction. Anisotropic electromagnetic material can be modeled as a set of electric and magnetic dipoles with an arbitrary ellipsoidal shape in vacuum. The tensor of an anisotropic material is denoted by two 3×3 Hermitian matrices. These matrices can be transformed to diagonal matrices using rotation of the coordinates system as

$$[\mu] = \begin{bmatrix} \mu_1 & 0 & 0 \\ 0 & \mu_2 & 0 \\ 0 & 0 & \mu_3 \end{bmatrix}; \quad [\varepsilon] = \begin{bmatrix} \varepsilon_1 & 0 & 0 \\ 0 & \varepsilon_2 & 0 \\ 0 & 0 & \varepsilon_3 \end{bmatrix} \tag{1}$$

These matrices are used for biaxial materials, with triclinic structures such as mineral examples including microcline ($KAlSi_3O_8$), plagioclase with $[\mu] = \mu_0 \mathrm{I}_3$ where I_3 is the 3×3 identity matrix. For uniaxial materials, such as the revolutionary ellipsoidal dipoles $\varepsilon_1 = \varepsilon_2$, $[\mu] = \mu_0 \mathrm{I}_3$, like Quartz. For spherical dipoles $\varepsilon_1 = \varepsilon_2 = \varepsilon_3$, $[\mu] = \mu_0 \mathrm{I}_3$ and $\overline{\overline{\varepsilon}}$ becomes a scalar, like Silicon and Gallium Arsenide [20]. Anisotropic magnetic materials are materials such as ferromagnetic materials including iron oxide (Feo_3), composites, ceramic ($BaO_6Fe_2O_3$), platinum cobalt (Pt, Co), cobalt samarium (Co, Sm) [21, 22]. For example [23]

$$[\mu] = \mu_0 \begin{bmatrix} 1.6664 - 0.0577i & 0.0532 + 0.4425i & 0 \\ -0.0532 - 0.4425i & 1.6664 - 0.0577i & 0 \\ 0 & 0 & 1 \end{bmatrix} \tag{2}$$

In this work, we use the MUSIC algorithm to find the locations of small electromagnetic inclusions with both μ and ε as complex scalars with an arbitrary ellipsoidal shape, within a noise-free or noisy homogeneous biaxial anisotropic permeable background medium, with scalar ε and second order tensor $[\mu]$. The inclusions take the form of $\mathcal{I}_\alpha = \cup_{j=1}^{m} \mathbf{z}_j + \alpha B_j$, where $B_j \subset \mathbb{R}^3$ and $\mathbf{z}_j \subset \mathbb{R}^3$ are the boundary and location of the jth inclusion, respectively, and α is the common order of magnitude of the inclusions dimensions as a small fraction of the wavelength. Let for dielectric inclusions $\mu_\alpha = \mu_0$, $\varepsilon_\alpha \neq \varepsilon_0$, for permeable inclusions $\mu_\alpha \neq \mu_0$, $\varepsilon_\alpha = \varepsilon_0$, for electromagnetic inclusions $\mu_\alpha \neq \mu_0$, $\varepsilon_\alpha \neq \varepsilon_0$, for combination of dielectric and permeable inclusions $\mu_\alpha \neq \mu_0$, $\varepsilon_\alpha = \varepsilon_0$ or $\mu_\alpha = \mu_0$, $\varepsilon_\alpha \neq \varepsilon_0$, and for background $[\mu_b] \neq \mu_0 \mathrm{I}_3$, $\varepsilon_b = \varepsilon_0$.

2. FORMULATION OF DIRECT PROBLEM

We firstly solve the direct problem. The inclusions are illuminated by several antennas, and then the scattered fields are evaluated as scattering matrix, A_α. The transmitting and receiving antennas are located in the constant z plane, $z = z_a$, with different (x_i, y_i), $i = 1, 2, \ldots, \sqrt{n}$. The inclusions are illuminated by transmitting antennas, and the scattered field is measured by all receiving antennas. In fact, we have mono/multi-static conditions. To find the locations of electromagnetic inclusions in an anisotropic permeable background as shown in Fig. 1 for the background, we have [24]

$$\begin{cases} \mathbf{B}_b = \mu_0 \left(\mathbf{H}_0^{(n)}(\mathbf{r}) \mathrm{I}_3 + \mathbf{M}_b \right) = \mu_0 \left(\mathbf{H}_0^{(n)}(\mathbf{r}) \mathrm{I}_3 + \overline{\overline{\chi}}_{m_b} \mathbf{H}_0^{(n)}(\mathbf{r}) \right) \\ \overline{\overline{\chi}}_{m_b} = \overline{\overline{\mu}}_{r_b} - \mathrm{I}_3 \\ \mathbf{M}_b = \left(\overline{\overline{\mu}}_{r_b} - \mathrm{I}_3 \right) \mathbf{H}_0^{(n)}(\mathbf{r}) = \overline{\overline{\rho}} \cdot \mathbf{H}_0^{(n)}(\mathbf{r}) \\ \overline{\overline{\rho}} = \left(\overline{\overline{\mu}}_{r_b} - \mathrm{I}_3 \right) \end{cases} \tag{3}$$

where $\overline{\overline{\chi}}_{m_b}$, $\overline{\overline{\mu}}_{r_b}$, and $\mathbf{M}_b$ are magnetic susceptibility, relative permeability tensor, and magnetization vector of the anisotropic magnetic background, respectively, and $\mathbf{H}_0^{(n)}(\mathbf{r})$ is the incident magnetic field at the position $\mathbf{r}$ due to the nth magnetic dipole element, directed in $\hat{\beta}_n$ as

$$\mathbf{M}_0^{(n)}(\mathbf{r}) = -i\omega\mu_0 \delta(\mathbf{r} - \mathbf{r}_n) \hat{\beta}_n Is \tag{4}$$

where constant Is is the magnetic moment. The incident electric field from the dual problem of the preceding problem is given in [17] as

$$\mathbf{E}_0^{(n)}(\mathbf{r}) = i\omega\mu_0 \left[\mathrm{I}_3 + \frac{\nabla\nabla}{k^2} \right] g\left(\mathbf{r}, \mathbf{r}'\right) \cdot \mathbf{J}_0^{(n)}(\mathbf{r}) \tag{5}$$

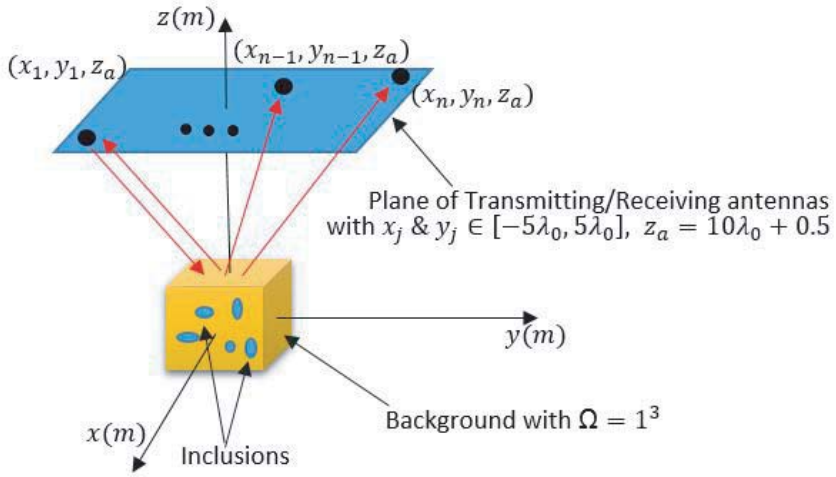

Figure 1. Configuration of the problem.

where $\mathbf{J}_0^{(n)}(\mathbf{r})$ is the current element, and

$$g\left(\mathbf{r},\mathbf{r}'\right) = \frac{e^{ik|\mathbf{r}-\mathbf{r}'|}}{4\pi|\mathbf{r}-\mathbf{r}'|} \tag{6}$$

is a scalar function. To obtain $\mathbf{H}_0^{(n)}(\mathbf{r})$, since partial differential equation of $\mathbf{H}_0^{(n)}(\mathbf{r})$ is the same as $\mathbf{E}_0^{(n)}(\mathbf{r})$, using duality theorem [17] it is enough that $\mathbf{E}$ by $\mathbf{H}$, $\mathbf{H}$ by $\mathbf{E}$, μ by $-\varepsilon$, ε by $-\mu$, and $\mathbf{J}$ by $-\mathbf{M}$ are replaced in Eq. (5)

$$\mathbf{H}_0^{(n)}(\mathbf{r}) = i\omega\varepsilon_0\left[\mathrm{I}_3 + \frac{\nabla\nabla}{k^2}\right] g\left(\mathbf{r},\mathbf{r}'\right)\cdot\mathbf{M}_0^{(n)}(\mathbf{r}) = k^2 Is\left[\mathrm{I}_3 + \frac{\nabla\nabla}{k^2}\right] g(\mathbf{r},\mathbf{r}_n)\cdot\hat{\beta}_n \tag{7}$$

We define the dyadic Green's function $\overline{\overline{\mathbf{G}}}$ as

$$\overline{\overline{\mathbf{G}}}\left(\mathbf{r},\mathbf{r}'\right) = \left[\mathrm{I}_3 + \frac{\nabla\nabla}{k^2}\right] g\left(\mathbf{r},\mathbf{r}'\right) \tag{8}$$

Using Eqs. (7) and (8), $\mathbf{H}_0^{(n)}(\mathbf{r})$ the scattered field at $\mathbf{r}$ due to $\mathbf{M}_0^{(n)}(\mathbf{r})$ at position of $\mathbf{r}_n$ is obtained as

$$\mathbf{H}_0^{(n)}(\mathbf{r}) = i\omega\varepsilon_0\overline{\overline{\mathbf{G}}}\left(\mathbf{r},\mathbf{r}'\right)\cdot\mathbf{M}_0^{(n)}(\mathbf{r}) = k^2 Is\,\overline{\overline{\mathbf{G}}}(\mathbf{r},\mathbf{r}_n)\cdot\hat{\beta}_n \tag{9}$$

By considering that $\nabla\times\mathbf{H}_0^{(n)}(\mathbf{r}) = -i\omega\varepsilon_0\mathbf{E}_0^{(n)}(\mathbf{r})$ we have

$$\mathbf{E}_0^{(n)}(\mathbf{r}) = i\omega\mu_0 Is\nabla\times\overline{\overline{\mathbf{G}}}(\mathbf{r},\mathbf{r}_n)\cdot\hat{\beta}_n \tag{10}$$

According to Eqs. (3) and (9), $\mathbf{M}_b(\mathbf{r})$ becomes

$$\mathbf{M}_b(\mathbf{r}) = k^2 Is\,\overline{\overline{\rho}}\cdot\overline{\overline{\mathbf{G}}}(\mathbf{r},\mathbf{r}_n)\cdot\hat{\beta}_n \tag{11}$$

Let $\mathbf{H}_b(\mathbf{r})$ be the scattered field at position of $\mathbf{r}$ due to $\mathbf{M}_b(\mathbf{r}')$, therefore

$$\mathbf{H}_b(\mathbf{r}) = i\omega\varepsilon_0\overline{\overline{\mathbf{G}}}\left(\mathbf{r},\mathbf{r}'\right)\cdot\mathbf{M}_b\left(\mathbf{r}'\right) = i\omega\varepsilon_0 k^2 Is\,\overline{\overline{\mathbf{G}}}\left(\mathbf{r},\mathbf{r}'\right)\cdot\overline{\overline{\rho}}\cdot\overline{\overline{\mathbf{G}}}\left(\mathbf{r}',\mathbf{r}_n\right)\cdot\hat{\beta}_n \tag{12}$$

$$\mathbf{E}_b(\mathbf{r}) = -\nabla\times\overline{\overline{\mathbf{G}}}\left(\mathbf{r},\mathbf{r}'\right)\cdot\mathbf{M}_b\left(\mathbf{r}'\right) = -k^2 Is\,\nabla\times\overline{\overline{\mathbf{G}}}\left(\mathbf{r},\mathbf{r}'\right)\cdot\overline{\overline{\rho}}\cdot\overline{\overline{\mathbf{G}}}\left(\mathbf{r}',\mathbf{r}_n\right)\cdot\hat{\beta}_n \tag{13}$$

Now $\mathbf{H}_b^{(n)}(\mathbf{r})$ is the scattered field at position of $\mathbf{r}$ due to $\mathbf{M}_0^{(n)}(\mathbf{r}_n)$ and $\mathbf{M}_b(\mathbf{r}')$ using Eqs. (9) and (12), hence

$$\mathbf{H}_b^{(n)}(\mathbf{r}) = \mathbf{H}_0^{(n)}(\mathbf{r}) + \mathbf{H}_b(\mathbf{r}) = k^2 Is\overline{\overline{\mathbf{G}}}(\mathbf{r},\mathbf{r}_n)\cdot\hat{\beta}_n + i\omega\varepsilon_0 k^2 Is\,\overline{\overline{\mathbf{G}}}\left(\mathbf{r},\mathbf{r}'\right)\cdot\overline{\overline{\rho}}\cdot\overline{\overline{\mathbf{G}}}\left(\mathbf{r}',\mathbf{r}_n\right)\cdot\hat{\beta}_n \tag{14}$$

$$\mathbf{E}_b^{(n)}(\mathbf{r}) = \mathbf{E}_0^{(n)}(\mathbf{r}) + \mathbf{E}_b(\mathbf{r}) = i\omega\mu_0 Is\nabla\times\overline{\overline{\mathbf{G}}}(\mathbf{r},\mathbf{r}_n)\cdot\hat{\beta}_n - k^2 Is\,\nabla\times\overline{\overline{\mathbf{G}}}\left(\mathbf{r},\mathbf{r}'\right)\cdot\overline{\overline{\rho}}\cdot\overline{\overline{\mathbf{G}}}\left(\mathbf{r}',\mathbf{r}_n\right)\cdot\hat{\beta}_n \tag{15}$$

Let $\mathbf{H}_{b+\alpha}^{(n)}$ be the total scattered fields at position of $\mathbf{r}$ due to $\mathbf{M}_0^{(n)}(\mathbf{r}_n)$, $\mathbf{M}_b(\mathbf{r}')$, and inclusions which satisfy

$$\begin{cases} \nabla \times \mathbf{E}_{b+\alpha}^{(n)} = i\omega \mathbf{B}_{b+\alpha}^{(n)} \\ \mathbf{B}_{b+\alpha}^{(n)} = \mu_0 \left(\mathbf{H}_{b+\alpha}^{(n)} + \mathbf{M}_b + \mathbf{M}_0^{(n)} \right) \\ \nabla \times \mathbf{H}_{b+\alpha}^{(n)} = \mathbf{J} - i\omega\varepsilon_\alpha \mathbf{E}_{b+\alpha}^{(n)}; \quad (\mathbf{J} = 0) \\ \nabla \times \mu_\alpha^{-1} \nabla \times \mathbf{H}_{b+\alpha}^{(n)} - \omega^2 \varepsilon_\alpha \mathbf{H}_{b+\alpha}^{(n)} = \omega^2 \varepsilon_\alpha \left(\mathbf{M}_b + \mathbf{M}_0^{(n)} \right) \end{cases} \tag{16}$$

For lossy inclusions we have $\varepsilon_\alpha = \varepsilon'_\alpha + j\varepsilon''_\alpha$ and $\mu_\alpha = \mu'_\alpha + j\mu''_\alpha$, where ε''_α and μ''_α are equal to zero for lossless inclusions. Multiplying Eq. (16) by $\overline{\overline{\mathbf{G}}}(\mathbf{r}', \mathbf{r}) \cdot \mathbf{a}$, where $\mathbf{a}$ is an arbitrary vector and integrating over volume V with boundary ∂V which contains all background and inclusions, we obtain

$$\begin{aligned} &\int_V d\mathbf{r}' \left[\nabla' \times \frac{1}{\mu_\alpha} \nabla' \times \mathbf{H}_{b+\alpha}^{(n)} \left(\mathbf{r}' \right) - \omega^2 \varepsilon_\alpha \mathbf{H}_{b+\alpha}^{(n)} \left(\mathbf{r}' \right) \right] \cdot \overline{\overline{\mathbf{G}}} \left(\mathbf{r}', \mathbf{r} \right) \cdot \mathbf{a} \\ = &\int_V d\mathbf{r}' \, \omega^2 \varepsilon_\alpha \left(\mathbf{M}_b \left(\mathbf{r}' \right) + \mathbf{M}_0^{(n)} \left(\mathbf{r}' \right) \right) \cdot \overline{\overline{\mathbf{G}}} \left(\mathbf{r}', \mathbf{r} \right) \cdot \mathbf{a} \end{aligned} \tag{17}$$

Then to obtain locations of electromagnetic inclusions, Equation (17) must be solved for scattered fields of them. For electromagnetic inclusions we have $\mu_\alpha \neq \mu_0$ and $\varepsilon_\alpha \neq \varepsilon_0$, so from Equation (17), Equation (17) becomes as [17]

$$\begin{aligned} &\int_V d\mathbf{r}' \left[\nabla' \times \frac{1}{\mu_\alpha} \nabla' \times \mathbf{H}_{b+\alpha}^{(n)} \left(\mathbf{r}' \right) - \omega^2 \varepsilon_\alpha \mathbf{H}_{b+\alpha}^{(n)} \left(\mathbf{r}' \right) \right] \cdot \overline{\overline{\mathbf{G}}} \left(\mathbf{r}', \mathbf{r} \right) \cdot \mathbf{a} \\ = &\oint_{\partial V} d\sigma n \cdot \frac{1}{\mu_0} \left[\nabla' \times \mathbf{H}_{b+\alpha}^{(n)} \left(\mathbf{r}' \right) \times \overline{\overline{\mathbf{G}}} \left(\mathbf{r}', \mathbf{r} \right) + \mathbf{H}_{b+\alpha}^{(n)} \left(\mathbf{r}' \right) \times \nabla' \times \overline{\overline{\mathbf{G}}} \left(\mathbf{r}', \mathbf{r} \right) \right] \cdot \mathbf{a} + \frac{1}{\mu_0} \mathbf{H}_{b+\alpha}^{(n)}(\mathbf{r}) \cdot \mathbf{a} \\ &+ \sum_{j=1}^{m} \int_{\mathbf{z}_j + \alpha B_j} d\mathbf{r}' \left[\left(\frac{1}{\mu_j} \mathrm{I}_3 - \overline{\overline{\mu}}_b^{-1} \right) \nabla' \times \mathbf{H}_{b+\alpha}^{(n)} \left(\mathbf{r}' \right) \cdot \nabla' \times \overline{\overline{\mathbf{G}}} \left(\mathbf{r}', \mathbf{r} \right) - \omega^2 (\varepsilon_j - \varepsilon_0) \cdot \mathbf{H}_{b+\alpha}^{(n)} \left(\mathbf{r}' \right) \cdot \overline{\overline{\mathbf{G}}} \left(\mathbf{r}', \mathbf{r} \right) \right] \cdot \mathbf{a} \\ = &\int_V d\mathbf{r}' \omega^2 \varepsilon_\alpha \left(\mathbf{M}_b \left(\mathbf{r}' \right) + \mathbf{M}_0^{(n)} \left(\mathbf{r}' \right) \right) \cdot \overline{\overline{\mathbf{G}}} \left(\mathbf{r}', \mathbf{r} \right) \cdot \mathbf{a} = \frac{\omega \varepsilon_\alpha}{i\varepsilon_0} \left(\mathbf{H}_b(\mathbf{r}) + \mathbf{H}_0^{(n)}(\mathbf{r}) \right) \cdot \mathbf{a} = \frac{\omega \varepsilon_\alpha}{i\varepsilon_0} \mathbf{H}_b^{(n)}(\mathbf{r}) \cdot \mathbf{a} \end{aligned} \tag{18}$$

where ε_α and μ_α are values of ε_j and μ_j at $\mathbf{z}_j$, and ∇', B_j, and $\mathbf{z}_j$ are the gradient operator with respect to variable $\mathbf{r}'$, the boundary of jth inclusion, and location of the jth inclusion, respectively. α is a small fraction of the wavelength at operating frequency. The first term of Eq. (18) is zero when V tends to be an infinite sphere because of the radiation condition. Therefore, we have

$$\begin{aligned} \mathbf{H}_{b+\alpha}^{(n)}(\mathbf{r}) - \frac{\omega \varepsilon_\alpha \mu_0}{i\varepsilon_0} \mathbf{H}_b^{(n)}(\mathbf{r}) = &\sum_{j=1}^{m} \int_{\mathbf{z}_j + \alpha B_j} d\mathbf{r}' \mu_0 \left[- \left(\frac{1}{\mu_j} \mathrm{I}_3 - \overline{\overline{\mu}}_b^{-1} \right) \nabla' \times \mathbf{H}_{b+\alpha}^{(n)} \left(\mathbf{r}' \right) \right. \\ &\left. \cdot \nabla' \times \overline{\overline{\mathbf{G}}} \left(\mathbf{r}', \mathbf{r} \right) + \omega^2 (\varepsilon_j - \varepsilon_0) \cdot \mathbf{H}_{b+\alpha}^{(n)} \left(\mathbf{r}' \right) \cdot \overline{\overline{\mathbf{G}}} \left(\mathbf{r}', \mathbf{r} \right) \right] \end{aligned} \tag{19}$$

Considering that $\nabla' \times \mathbf{H}_{b+\alpha}^{(n)}(\mathbf{r}') = -i\omega\varepsilon(\mathbf{r}') \mathbf{E}_{b+\alpha}^{(n)}(\mathbf{r}')$ where $\varepsilon(\mathbf{r}') = \varepsilon_0$ if $\mathbf{r}' \neq \mathbf{z}_j$ and $\varepsilon(\mathbf{r}') = \varepsilon_j$ if $\mathbf{r}' = \mathbf{z}_j$, we have

$$\begin{aligned} \mathbf{H}_{b+\alpha}^{(n)}(\mathbf{r}) - \frac{\omega \varepsilon_\alpha \mu_0}{i\varepsilon_0} \mathbf{H}_b^{(n)}(\mathbf{r}) = &\sum_{j=1}^{m} \int_{\mathbf{z}_j + \alpha B_j} d\mathbf{r}' \left[-i\omega\varepsilon \left(\mathbf{r}' \right) \mu_0 \left(\frac{1}{\mu_j} \mathrm{I}_3 - \overline{\overline{\mu}}_b^{-1} \right) \cdot \nabla' \right. \\ &\left. \times \overline{\overline{\mathbf{G}}} \left(\mathbf{r}, \mathbf{r}' \right) \cdot \mathbf{E}_{b+\alpha}^{(n)} \left(\mathbf{r}' \right) + \mu_0 \omega^2 (\varepsilon_j - \varepsilon_0) \cdot \overline{\overline{\mathbf{G}}} \left(\mathbf{r}, \mathbf{r}' \right) \cdot \mathbf{H}_{b+\alpha}^{(n)} \left(\mathbf{r}' \right) \right] \end{aligned} \tag{20}$$

We use expressions of far fields because the transmitters, receivers and background containing inclusions are in the far-field region.

3. FAR-FIELD EXPRESSIONS FOR DIRECT PROBLEM

For $\overline{\overline{\mathbf{G}}}(\mathbf{r},\mathbf{r}')$ and $\nabla'\times\overline{\overline{\mathbf{G}}}(\mathbf{r},\mathbf{r}')$, we define far-field pattern by $\Lambda(\mathbf{r})$ and $\Delta(\mathbf{r})$ matrices as [17]

$$\begin{cases}\overline{\overline{\mathbf{G}}}(\mathbf{r},\mathbf{r}')=\dfrac{e^{ikr}}{4\pi r}e^{-ik\hat{\mathbf{r}}\cdot\mathbf{r}'}\Delta(\mathbf{r})\\ \nabla'\times\overline{\overline{\mathbf{G}}}(\mathbf{r},\mathbf{r}')=-ik\dfrac{e^{ikr}}{4\pi r}e^{-ik\hat{\mathbf{r}}\cdot\mathbf{r}'}\Lambda(\mathbf{r})\end{cases}\tag{21}$$

where

$$\Delta(\mathbf{r})=\Lambda(\mathbf{r})\Lambda^T(\mathbf{r})\tag{22}$$

where T is the transpose, and

$$\Lambda(\mathbf{r})=\begin{bmatrix}0 & -\hat{\mathbf{r}}_z & \hat{\mathbf{r}}_y\\ \hat{\mathbf{r}}_z & 0 & -\hat{\mathbf{r}}_x\\ -\hat{\mathbf{r}}_y & \hat{\mathbf{r}}_x & 0\end{bmatrix}\tag{23}$$

because of $\Lambda^T(\mathbf{r})=-\Lambda(\mathbf{r})$, so $\Delta^T(\mathbf{r})=\Delta(\mathbf{r})$. We have

$$\begin{cases}\overline{\overline{\mathbf{G}}}(\mathbf{r}_n,\mathbf{r})=\left[\overline{\overline{\mathbf{G}}}(\mathbf{r},\mathbf{r}_n)\right]^T=\overline{\overline{\mathbf{G}}}(\mathbf{r},\mathbf{r}_n)\\ \nabla\times\overline{\overline{\mathbf{G}}}(\mathbf{r},\mathbf{r}_n)=\left[\nabla'\times\overline{\overline{\mathbf{G}}}(\mathbf{r}_n,\mathbf{r})\right]^T=-\nabla'\times\overline{\overline{\mathbf{G}}}(\mathbf{r}_n,\mathbf{r})\end{cases}\tag{24}$$

By some of mathematical manipulations we have

$$\begin{cases}-\hat{\mathbf{r}}\times(\hat{\mathbf{r}}\times\mathbf{a})=\Delta(\mathbf{r})\cdot\mathbf{a}\\ \hat{\mathbf{r}}\times\mathbf{a}=\Lambda(\mathbf{r})\cdot\mathbf{a}\end{cases}\tag{25}$$

For $\overline{\overline{\mathbf{G}}}(\mathbf{r},\mathbf{r}_n)$ and $\nabla'\times\overline{\overline{\mathbf{G}}}(\mathbf{r},\mathbf{r}_n)$ in the far-field region we have

$$\begin{cases}\overline{\overline{\mathbf{G}}}(\mathbf{r},\mathbf{r}_n)\cdot\mathbf{a}=-\dfrac{e^{ikr}}{4\pi r}e^{-ik\hat{\mathbf{r}}\cdot\mathbf{r}_n}\hat{\mathbf{r}}\times(\hat{\mathbf{r}}\times\mathbf{a})\\ \nabla'\times\overline{\overline{\mathbf{G}}}(\mathbf{r},\mathbf{r}_n)\cdot\mathbf{a}=-ik\dfrac{e^{ikr}}{4\pi r}e^{-ik\hat{\mathbf{r}}\cdot\mathbf{r}_n}\hat{\mathbf{r}}\times\mathbf{a}\end{cases}\tag{26}$$

Using Eqs. (9) and (25) in the far-field region of current element $\mathbf{M}_0^{(n)}(\mathbf{r})$ produces $\mathbf{H}_0^{(n)}(\mathbf{r})$ as

$$\mathbf{H}_0^{(n)}(\mathbf{r})=-k^2Is\,\hat{\mathbf{r}}_n\times\left(\hat{\mathbf{r}}_n\times\hat{\beta}_n\right)e^{-ik\hat{\mathbf{r}}_n\cdot\mathbf{r}}=k^2Is\,e^{-ik\hat{\mathbf{r}}_n\cdot\mathbf{r}}\Delta(\mathbf{r}_n)\cdot\hat{\beta}_n\tag{27}$$

Therefore, $\mathbf{M}_b(\mathbf{r}')$ from Eq. (11) becomes

$$\mathbf{M}_b\left(\mathbf{r}'\right)=k^2Is\,e^{-ik\hat{\mathbf{r}}_n\cdot\mathbf{r}'}\overline{\overline{\rho}}\cdot\Delta(\mathbf{r}_n)\cdot\hat{\beta}_n\tag{28}$$

Then from Eqs. (14) and (15) for $\mathbf{H}_b^{(n)}(\mathbf{r}')$ and $\mathbf{E}_b^{(n)}(\mathbf{r}')$ we have

$$\mathbf{H}_b^{(n)}\left(\mathbf{r}'\right)=k^2Ise^{-ik\hat{\mathbf{r}}_n\cdot\mathbf{r}'}\Delta(\mathbf{r}_n)\cdot\left(\mathrm{I}_3+i\omega\varepsilon_0e^{-ik\hat{\mathbf{r}}'\cdot\mathbf{r}'}\overline{\overline{\rho}}\cdot\Delta\left(\mathbf{r}'\right)\right)\cdot\hat{\beta}_n\tag{29}$$

$$\mathbf{E}_b^{(n)}\left(\mathbf{r}'\right)=k^2Ise^{-ik\hat{\mathbf{r}}_n\cdot\mathbf{r}'}\left(\omega\mu_0\Lambda(\mathbf{r}_n)+ike^{-ik\hat{\mathbf{r}}'\cdot\mathbf{r}'}\overline{\overline{\rho}}\cdot\Delta(\mathbf{r}_n)\cdot\Lambda\left(\mathbf{r}'\right)\right)\cdot\hat{\beta}_n\tag{30}$$

4. POLARIZATION TENSORS

If volume B_j (volume of the jth inclusion) is an ellipsoid with equation of

$$\frac{x_1^2}{a^2}+\frac{x_2^2}{b^2}+\frac{x_3^2}{c^2}=1,\quad 0<c\le b\le a\tag{31}$$

then its polarization tensor $\mathbf{M}_i(K;B_j)$ has the following form [25]

$$\mathbf{M}_i\left(K;B_j\right)=(K-1)|B_j|\begin{bmatrix}\frac{1}{(1-A)+KA} & 0 & 0\\ 0 & \frac{1}{(1-B)+KB} & 0\\ 0 & 0 & \frac{1}{(1-C)+KC}\end{bmatrix}\tag{32}$$

where K is $\frac{\varepsilon_j}{\varepsilon_0}$ for dielectric and $\frac{\mu_j}{\mu_0}$ for permeable inclusions, and A, B and C are defined as

$$\begin{cases} A = \dfrac{bc}{a^2}\displaystyle\int_1^{+\infty} \dfrac{1}{t^2\sqrt{t^2-1+\left(\frac{b}{a}\right)^2}\sqrt{t^2-1+\left(\frac{c}{a}\right)^2}}dt \\ B = \dfrac{bc}{a^2}\displaystyle\int_1^{+\infty} \dfrac{1}{\left(t^2-1+\left(\frac{b}{a}\right)^2\right)^{\frac{3}{2}}\sqrt{t^2-1+\left(\frac{c}{a}\right)^2}}dt \\ C = \dfrac{bc}{a^2}\displaystyle\int_1^{+\infty} \dfrac{1}{\sqrt{t^2-1+\left(\frac{b}{a}\right)^2}\left(t^2-1+\left(\frac{c}{a}\right)^2\right)^{\frac{3}{2}}}dt \end{cases} \tag{33}$$

In the following asymptotic formulation in accordance with [17], we use expressions far-field and polarization tensor.

5. ASYMPTOTIC FORMULA OF DIRECT PROBLEM FOR ELECTROMAGNETIC INCLUSIONS

For any $\mathbf{r}$ away from $\mathbf{r}_n$ and $\mathbf{z}_j$, $j = 1, \ldots, m$, Equation (20) using results of [17] gives

$$\begin{aligned} \mathbf{H}_{b+\alpha}^{(n)}(\mathbf{r}) - \frac{\omega\varepsilon_\alpha\mu_0}{i\varepsilon_0}\mathbf{H}_b^{(n)}(\mathbf{r}) \;=\; & \alpha^3\sum_{j=1}^{m}\left[-i\omega\varepsilon_j\mu_0\left(\frac{1}{\mu_j}\mathrm{I}_3 - \overline{\overline{\mu}}_b^{-1}\right)\cdot\nabla'\times\overline{\overline{\mathbf{G}}}(\mathbf{r},\mathbf{z}_j)\cdot\mathbf{M}_i\left(\frac{\mu_j}{\mu_0};B_j\right)\cdot\mathbf{E}_b^{(n)}(\mathbf{z}_j)\right. \\ & \left.+\mu_0\omega^2(\varepsilon_j-\varepsilon_0)\cdot\overline{\overline{\mathbf{G}}}(\mathbf{r},\mathbf{z}_j)\cdot\mathbf{M}_i\left(\frac{\varepsilon_j}{\varepsilon_0};B_j\right)\cdot\mathbf{H}_b^{(n)}(\mathbf{z}_j)\right] \end{aligned} \tag{34}$$

Using Eqs. (21), (29) and (30) for $\nabla'\times\overline{\overline{\mathbf{G}}}(\mathbf{r},\mathbf{z}_j)$, $\overline{\overline{\mathbf{G}}}(\mathbf{r},\mathbf{z}_j)$, $\mathbf{H}_b^{(n)}(\mathbf{z}_j)$ and $\mathbf{E}_b^{(n)}(\mathbf{z}_j)$ to substitute in Eq. (34), we have

$$\begin{aligned} \mathbf{H}_{b+\alpha}^{(n)}(\mathbf{r}) - \frac{\omega\varepsilon_\alpha\mu_0}{i\varepsilon_0}\mathbf{H}_b^{(n)}(\mathbf{r}) \;=\; & \alpha^3k^2Is\frac{e^{ikr}}{4\pi r}\sum_{j=1}^{m}e^{-ik\hat{\mathbf{r}}_n\cdot\mathbf{z}_j}e^{-ik\hat{\mathbf{r}}\cdot\mathbf{z}_j}\left[-i\omega\varepsilon_jk\mu_0\left(\frac{1}{\mu_j}\mathrm{I}_3-\overline{\overline{\mu}}_b^{-1}\right)\cdot\Lambda(\mathbf{r})\right. \\ & \cdot\mathbf{M}_i\left(\frac{\mu_j}{\mu_0};B_j\right)\cdot\{\omega\mu_0\Lambda(\mathbf{r}_n)+ike^{-ik\hat{\mathbf{z}}_j\cdot\mathbf{z}_j}\overline{\overline{\rho}}\cdot\Delta(\mathbf{r}_n)\cdot\Lambda(\mathbf{z}_j)\}+\omega^2\mu_0(\varepsilon_j-\varepsilon_0) \\ & \left.\cdot\Delta(\mathbf{r})\cdot\mathbf{M}_i\left(\frac{\varepsilon_j}{\varepsilon_0};B_j\right)\cdot\{\mathrm{I}_3+i\omega\varepsilon_0e^{-ik\hat{\mathbf{z}}_j\cdot\mathbf{z}_j}\,\overline{\overline{\rho}}\cdot\Delta(\mathbf{z}_j)\}\cdot\Delta(\mathbf{r}_n)\right]\cdot\hat{\beta}_n \end{aligned} \tag{35}$$

where $A_\alpha(\hat{\mathbf{r}},\hat{\mathbf{r}}_n)$ is the scattered field amplitude from the inclusions. The function $A_\alpha(\hat{\mathbf{r}},\hat{\mathbf{r}}_n)$ can be expanded as [17]

$$\mathbf{H}_{b+\alpha}^{(n)}(\mathbf{r}) = \frac{\omega\varepsilon_\alpha\mu_0}{i\varepsilon_0}\mathbf{H}_b^{(n)}(\mathbf{r}) + A_\alpha\left(\hat{\mathbf{r}},\hat{\mathbf{r}}_n\right)\frac{e^{ikr}}{4\pi r} + O\left(\frac{1}{r^2}\right) \tag{36}$$

For arbitrary directions of transmitter and receiver antennas $\hat{\beta}_n$, $\hat{\xi}$ at positions of $\hat{\mathbf{r}}_n$ and $\mathbf{r}$, respectively, for $A_\alpha(\hat{\mathbf{r}},\hat{\mathbf{r}}_n)$, we have

$$\begin{aligned} \hat{\xi}_p\cdot A_\alpha\left(\hat{\mathbf{r}},\hat{\mathbf{r}}_n\right) \;=\; & \alpha^3k^2Is\sum_{j=1}^{m}e^{-ik\hat{\mathbf{r}}_n\cdot\mathbf{z}_j}e^{-ik\hat{\mathbf{r}}\cdot\mathbf{z}_j}\hat{\xi}_p\cdot\left[-i\omega\varepsilon_jk\left(\mathrm{I}_3-\mu_0\overline{\overline{\mu}}_b^{-1}\right)\cdot\Lambda(\mathbf{r})\right. \\ & \cdot\mathbf{M}_i\left(\frac{\mu_j}{\mu_0};B_j\right)\cdot\{\omega\mu_0\Lambda(\mathbf{r}_n)+ike^{-ik|\mathbf{z}_j|}\overline{\overline{\rho}}\cdot\Delta(\mathbf{r}_n)\cdot\Lambda(\mathbf{z}_j)\}+\omega^2\mu_0(\varepsilon_\alpha-\varepsilon_0)\cdot\Delta(\mathbf{r}) \\ & \left.\cdot\mathbf{M}_i\left(\frac{\varepsilon_j}{\varepsilon_0};B_j\right)\cdot\{\mathrm{I}_3+i\omega\varepsilon_0e^{-ik|\mathbf{z}_j|}\overline{\overline{\rho}}\cdot\Delta(\mathbf{z}_j)\}\cdot\Delta(\mathbf{r}_n)\right]\cdot\hat{\beta}_n \end{aligned} \tag{37}$$

From Eq. (37), we calculate scattered fields for direct problem and then obtain locations of inclusions by solving inverse problem using MUSIC algorithm as following.

6. THE MUSIC ALGORITHM

In inverse problem, we find locations of inclusions from scattered fields of amplitude matrices A_α of them using MUSIC algorithm. Let the Singular Value Decomposition (SVD) of the matrix A_α, for the same number of transmitting and receiving antennas, be denoted by $A_\alpha = \mathbf{U}\Sigma\mathbf{W}^*$ where Σ is an $n \times n$ diagonal matrix with non-negative real numbers entries. The diagonal entries σ_i, $i = 1, \ldots, n$ of Σ are known as the singular values of A_α. The orthogonal projections null space of A_α is given by [17]

$$\mathbf{P}_{\text{noise}} = \mathrm{I} - (\mathbf{U}_S \mathbf{U}_S^*) \tag{38}$$

where $S = 1, \ldots, 5m$ for dielectric inclusions, $S = 1, \ldots, 2m$ for permeable inclusions, $S = 1, \ldots, 5m$ for electromagnetic inclusions. m is the number of inclusions, and $\mathbf{U}_S$ is the Sth column of $\mathbf{U}$. A test point $\mathbf{z}$ coincides with one of the positions of inclusions, $\mathbf{z}_j$ if and only if $\mathbf{P}_{\text{noise}}(\mathbf{g} \cdot \mathbf{a}) = 0$ or

$$\mathrm{W}(\mathbf{z}) = \frac{1}{||\mathbf{P}_{\text{noise}}(\mathbf{g} \cdot \mathbf{a})||} = \infty \tag{39}$$

where for same directions of transmitter and receiver antennas ($\hat{\beta}_n = \hat{\beta}$ and $\hat{\xi}_p = \hat{\xi}$), $\mathbf{g}$ is

$$\mathbf{g} = \left(e^{-ik\hat{\mathbf{R}}_1 \cdot \mathbf{z}} \Lambda(\mathbf{R}_1) \cdot \hat{\xi}, \ldots, e^{-ik\hat{\mathbf{R}}_p \cdot \mathbf{z}} \Lambda(\mathbf{R}_p) \cdot \hat{\xi} \right), \quad p = 1, \ldots, n \tag{40}$$

where $\Lambda(\mathbf{R}_p)$ is defined in Eq. (23), and $\widehat{\mathbf{R}}_p$ is a unit vector in direction of $\mathbf{R}_p$, the location of Pth receiver antennas. n is the number of transmitter antennas and $\mathbf{a}$ an arbitrary vector.

7. NUMERICAL RESULTS

In this section, we first solve the direct problem by evaluation of the scattering matrix A_α from Eq. (37), then $\mathbf{U}_S$ is obtained from SVD of A_α. Locations of the inclusions are found using computation of $\mathrm{W}(\mathbf{z})$ according to the MUSIC algorithm, so that wherever $\mathrm{W}(\mathbf{z})$ becomes a very large number, that is the location of one inclusion. The numerical results of electromagnetic inclusions located in a permeable anisotropic background using MUSIC algorithm are presented. This algorithm is used for transmitting and receiving antennas placed in $\mathbf{r}_n = \mathbf{R}_p$ in the $z = z_a$ plane as shown in Figure 1. The frequency is 1 GHz, $z_a = 10\lambda_0 + 0.05$, and the ith transmitting and receiving antenna is at $x = -5\lambda_0 + \frac{10}{\sqrt{n}-1}(i-1)\lambda_0$ and $y = -5\lambda_0 + \frac{10}{\sqrt{n}-1}(j-1)\lambda_0$ for $i, j = 1, \ldots, \sqrt{n}$. Also, permeability tensor of the background, $\overline{\overline{\mu}}_{r_b}$, is chosen as

$$[\mu_{\mathrm{r}_b}] = \begin{bmatrix} 0.829 & -0.544i & 0 \\ 0.544i & 0.829 & 0 \\ 0 & 0 & 1 \end{bmatrix} \tag{41}$$

Then, the diagonal form of $\overline{\overline{\mu}}_{\mathrm{r}_b}$ is obtained as, $\overline{\overline{\mu}}_{r_b} = 10^{-5}\mathrm{diag}[0.0358, 0.1257, 0.1725]$. Also, $k1 = \omega\sqrt{\mu_{r_{bxx}}\varepsilon_0\mu_0}$ and $\lambda_1 = 2\pi/\mathrm{Re}(k_1) = 0.5617\,\mathrm{m}$, $a = 0.25\lambda_1$, $b = 0.18\lambda_1$, $c = 0.1\lambda_1$ in Equation (31), and $\alpha = 0.1\lambda_1$ in Equations (18) and (37).

The number of singular values of A_α is equal to the number of transmitting or receiving antennas, but it is not necessary to consider all of them. It is enough to consider several of them that are bigger. Because A_α is compacted it has limitedness of the degrees of freedom for scattered fields. Therefore, it can affect the number of transmitting/receiving antennas. The number of transmitting/receiving antennas must satisfy $k\Omega + 1$ where Ω is the dimension of background and $k = \frac{2\pi}{\lambda_0}$ [26]. We assume that the background is surrounded by a cube with side length 1 m. In this case, the background dimension becomes $\Omega = 1.7321$. Therefore for frequency range 1–29 GHz, we need $n = 38$–1053 transmitting/receiving antennas, so we choose $n = 7^2$ for 1 GHz and $n = 34^2$ for 29 GHz.

To find locations of the ellipsoid inclusions, the parameters are chosen as $\hat{\beta}_n = [1\,;0\,;0]$, $\hat{\xi} = \hat{\beta}_n^T$ and $\mathbf{a} = [1, 1, 1]$. The results of simulations are for A_α which is polluted by Additive White Gaussian Noise,

AWGN, with 5 dB Signal to Noise Ratios, SNR. In some radars, SNR varies from -25 to 15 dB [27] and in DF (Direction Finding) is of order 5 dB [28], so we assume typical practical values $S = -120$ dBm, bandwidth range from 1–200 kHz for thermal noise as $N = kTB$, $k = 1.3810^{-23}\frac{J}{K}$, $T = 290$ K; therefore, the SNR range is 1–24 dB. We choose typical SNR = 5 dB. For real world application, the background may be Cobalt Samarium alloys [29] and inclusions as impurities and AWGN as thermal noise of ambient.

In this work, as some examples, locations of 5 isotropic ellipsoid inclusions in the anisotropic medium are found for five cases as follows:

Table 1. Assumed locations of inclusions for the above seven cases ($\lambda_0 = 0.3$ (m)).

Locations→ Case↓	$\mathbf{z}_1$ (m)	$\mathbf{z}_2$ (m)	$\mathbf{z}_3$ (m)	$\mathbf{z}_4$ (m)	$\mathbf{z}_5$ (m)
1	$[-0.4, 0, 0.4]$	$[0.4, -0.4, -0.4]$	$[0.1, 0.4, 0.16]$	$[-0.1, 0.1, 0]$	$[0.3, -0.3, 0]$
2	$[-0.4, -0.4, -0.4]$	$[0.1, 0.2, -0.44]$	$[-0.3, 0.3, -0.1]$	$[0, 0, 0]$	$[0.3, -0.1, -0.1]$
3	$[0.4, -0.4, -0.4]$	$[0.1, 0.4, 0.16]$	$[0.2, 0.4, -0.46]$	$[-0.1, -0.3, 0.46]$	$[-0.4, -0.2, -0.3]$
4	$[-0.1, 0.1, 0.44]$	$[0.45, -0.4, 0.26]$	$[0.2, -0.3, -0.28]$	$[-0.2, 0.4, -0.48]$	$[-0.45, 0, -0.4]$
5	$[0, 0.4, 0.26]$	$[0.1, -0.3, 0]$	$[0.2, -0.2, -0.26]$	$[0.3, 0.1, 0.34]$	$[-0.4, -0.4, -0.18]$

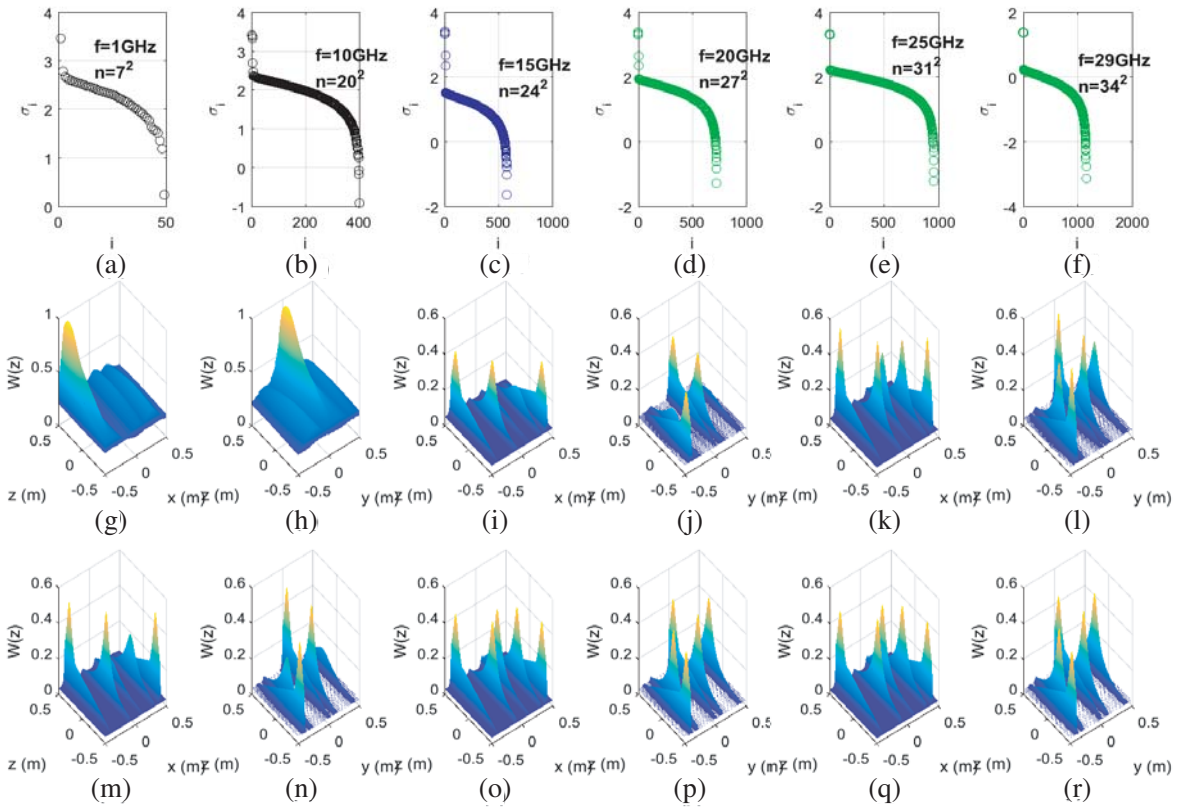

Figure 2. The case 1_1. (a) to (f) The singular values of A_α in the noisy background with SNR = 5 dB, $f = [1, 10, 15, 20, 25, 29]$ GHz, and $n = [7^2, 24^2, 24^2, 24^2, 24^2, 24^2]$, respectively. (g) & (h) Locating of inclusions in $f = 1$ GHz and $n = 7^2$. (i) & (j) Locating of inclusions in $f = 10$ GHz and $n = 20^2$. (k) & (l) Locating of inclusions in $f = 15$ GHz and $n = 24^2$. (m) & (n) Locating of inclusions in $f = 20$ GHz and $n = 27^2$. (o) & (p) Locating of inclusions in $f = 25$ GHz and $n = 31^2$. (q) & (r) Locating of inclusions in $f = 29$ GHz and $n = 34^2$.

1. For dielectric inclusions ($\varepsilon_j \neq \varepsilon_0$ and $\mu_j = \mu_0$).
   Cases 1_1 to case 1_4 are seven examples for case 1 as Table 2.
2. For permeable inclusions ($\varepsilon_j = \varepsilon_0$ and $\mu_j \neq \mu_0$).
3. For lossless electromagnetic inclusions ($\varepsilon_j \neq \varepsilon_0$ and $\mu_j \neq \mu_0$).
4. For lossy electromagnetic inclusions ($\varepsilon_j \neq \varepsilon_0$ and $\mu_j \neq \mu_0$).

Table 2. Several examples for the cases 1–5 of Table 2.

Case→ Material↓	1_1	1_2	1_3	1_4	2	3	4	5
ε_{r_1}	12	12	10	1.1	1	3	5	4
ε_{r_2}	1.5	11	10	1.1	1	5	$1.1i$	1
ε_{r_3}	2	2	10	1.1	1	7	$2.5+3i$	3
ε_{r_4}	1.1	10	10	1.1	1	4	$2.5i$	$5i$
ε_{r_5}	3	3	10	1.1	1	8	$4i$	1
μ_{r_1}	1	1	1	1	1.1	3	$3+2i$	1
μ_{r_2}	1	1	1	1	100	6	$2i$	1.1
μ_{r_3}	1	1	1	1	4	7	$7i$	3
μ_{r_4}	1	1	1	1	1.5	4	$4+i$	$3+2i$
μ_{r_5}	1	1	1	1	5	2	$2i$	$5i$

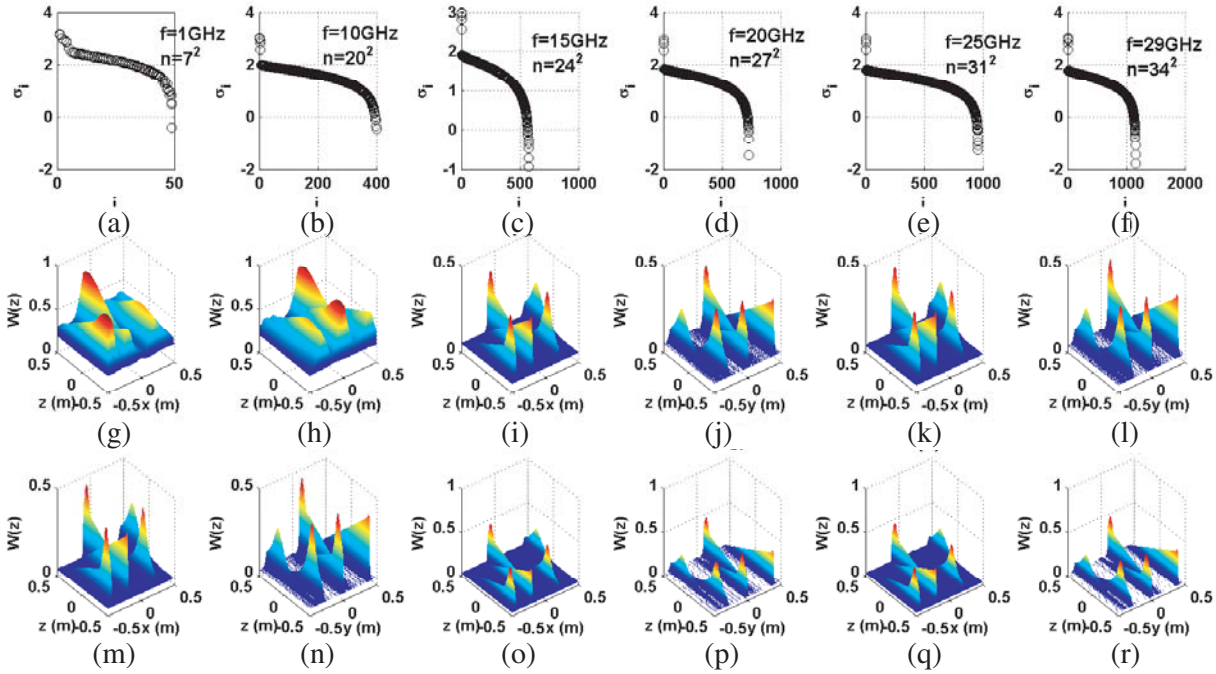

Figure 3. The case 4. (a) to (f) The singular values of A_α in the noisy background with SNR = 5 dB, $f = [1, 10, 15, 20, 25, 29]$ GHz, and $n = [7^2, 24^2, 24^2, 24^2, 24^2, 24^2]$, respectively. (g) & (h) Locating of inclusions in $f = 1$ GHz and $n = 7^2$. (i) & (j) Locating of inclusions in $f = 10$ GHz and $n = 7^2$. (k) & (l) Locating of inclusions in $f = 15$ GHz and $n = 7^2$. (m) & (n) Locating of inclusions in $f = 20$ GHz and $n = 7^2$. (o) & (p) Locating of inclusions in $f = 25$ GHz and $n = 7^2$. (q) & (r) Locating of inclusions in $f = 30$ GHz and $n = 24^2$.

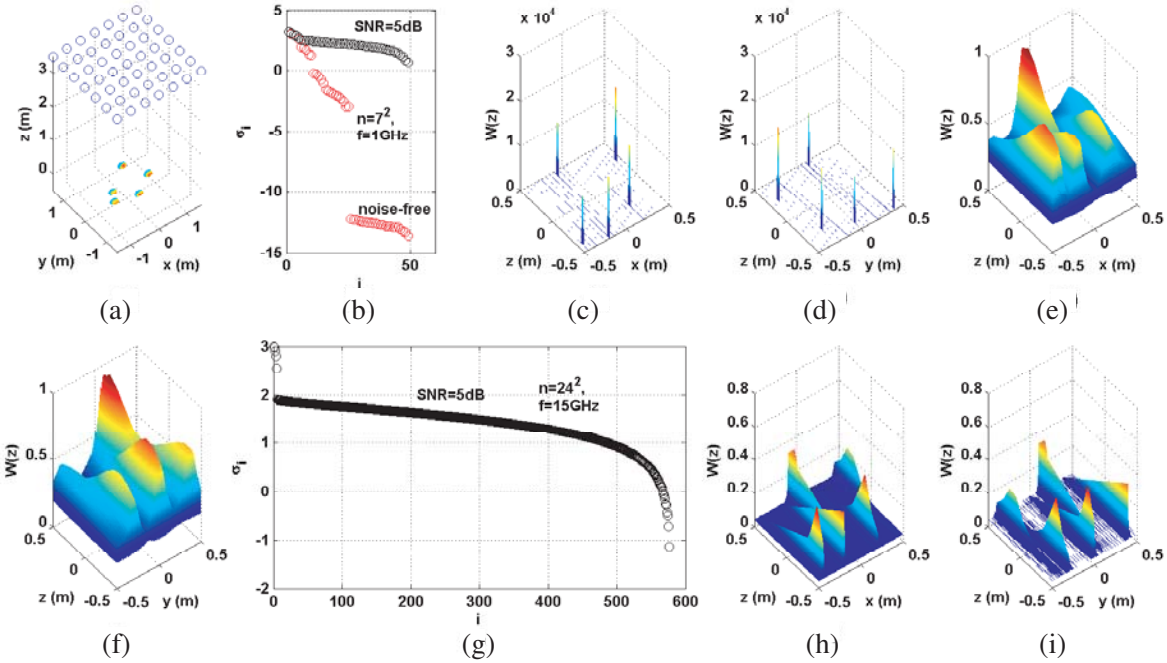

Figure 4. The case 4. (a) Random locations of inclusions in 3D. (b) The singular values of A_α in a noise-free and a noisy background with $n = 7^2$, SNR $= 5\,$dB, and $f = 1\,$GHz. (c) The locations of the lossy electromagnetic inclusions in a noise-free background in x-z plane for $f = 1\,$GHz. (d) The locations of the lossy electromagnetic inclusions in a noise-free background in y-z plane for $f = 1\,$GHz. (e) The locations of the lossy electromagnetic inclusions in a noisy background with SNR $= 5\,$dB in x-z plane for $f = 1\,$GHz. (f) The locations of the lossy electromagnetic inclusions in a noisy background with SNR $= 5\,$dB in y-z plane for $f = 1\,$GHz. (g) The singular values of A_α in a noise-free and a noisy background with $n = 24^2$, SNR $= 5\,$dB, and $f = 15\,$GHz. (h) The locations of the lossy electromagnetic inclusions in a noisy background with SNR $= 5\,$dB in x-z plane for $f = 15\,$GHz. (i) The locations of the lossy electromagnetic inclusions in a noisy background with SNR $= 5\,$dB in y-z plane for $f = 15\,$GHz.

5. For some combinations of the previous cases.

The locations inclusions for different cases are assumed as in Table 1, and materials of inclusions for different examples of cases are as considered in Table 2.

By increasing the frequency to 29 GHz, we simulate case 1_1 and case 4, and the results are shown in Figures 2 and 3.

We have shown results of, case 1_1 in Figure 2, and case 4 with random locations in Figures 3 and 4.

At the end, we have investigated the proposed formulation for the extended targets. As shown in Figure 5, two separate magnetic circles with $\mu = 2\mu_0$, $\varepsilon = \varepsilon_0$ are retrieved that are placed in plane $z = 0.2\,$m and $z = -0.2\,$m. Each target is extended by 10 point scatterers. Two separate circles or two extended targets, one times in a noise-free and the other time in a noisy background with SNR $= 5\,$dB, are shown in Figure 5.

Finally some cases are selected from Table 2 for simulation as in Table 3.

Description for Table 3: In all cases, the differences between singular values A_α for a noise-free background are very considerable, and all of the inclusions are restored.

In these figures, for solving Eq. (38), we consider Eq. (38) $S = 1, \ldots, m$ or $5m$ that means the first m or $5m$ columns of $\mathbf{U}$ matrix are enough to be considered as columns of $\mathbf{P}_{\text{noise}}$ in Equation (38). These columns span the range A_α or signal subspace, and the remainder span null or noise subspace. Singular values of A_α for signal subspace have larger values than null or noise subspace. It is observed from Figure 2 that $\mathrm{W}(\mathbf{z})$ is a large number of order of magnitude 4 for a noise-free background, when

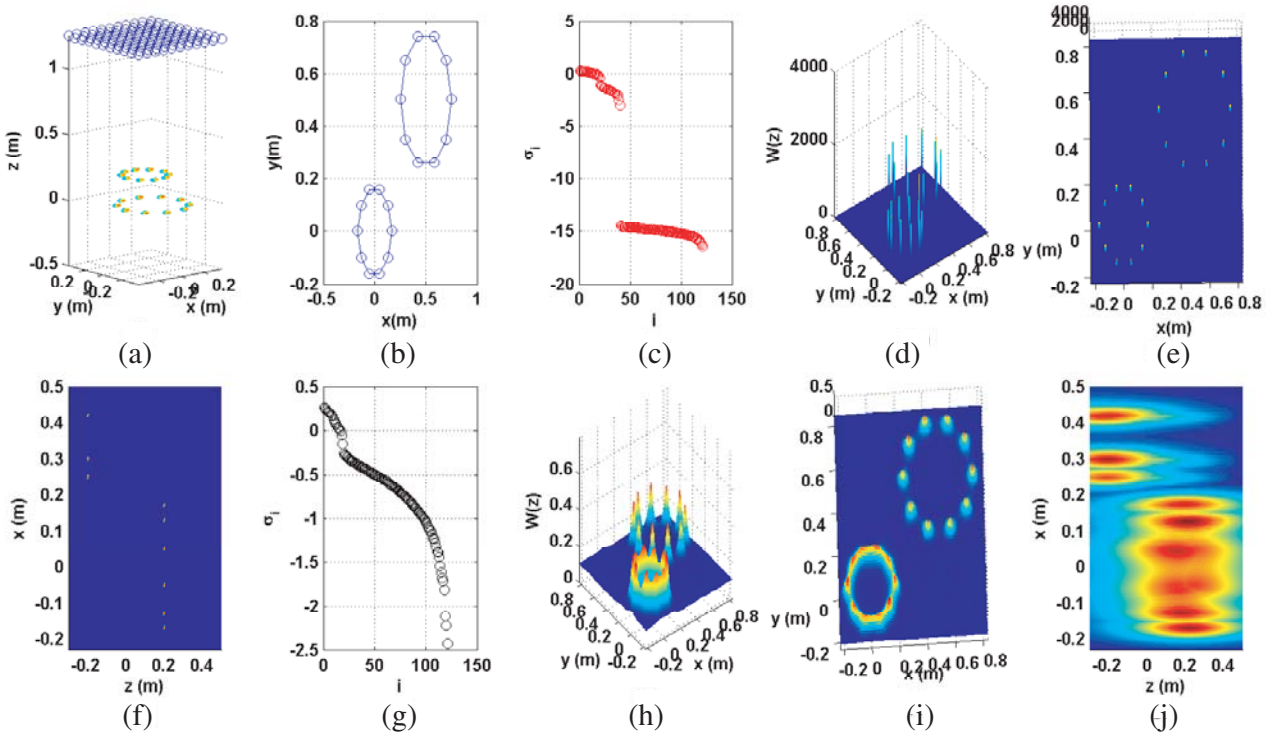

Figure 5. The extended targets for $n = 11^2$ and $f = 4\,\text{GHz}$. (a) Locations of extended targets in 3D. (b) Locations of extended targets in 2D. ((c) The singular values of A_α in a noise-free background. (d), (e), & (f) The locations of extended targets in a noise-free background. (f) The singular values of A_α in a noisy background SNR = 5. (h), (i), & (j) The locations of extended targets in a noisy background with SNR = 5 dB.

Table 3. The results of simulation of all cases in Tables 2 and 3 are as following: (for $f = 1\,\text{GHz}$, $m = 5$ (number of inclusions), and $n = 7^2$ (number of transmitting/receiving antennas).

condition→ case↓	Difference between singular values A_α for SNR = 5 dB	signal subspace for nois-free	signal subspace for SNR = 5 dB	locating of inclusions for SNR = 5 dB
1_1	very low	$5m(=25)$	1	just $\varepsilon_j = 12$
1_2	very low	$5m(=25)$	3	just $\varepsilon_j = [12, 11, 10]$
1_3 & 1_4	considerable	$5m(=25)$	5	all of them
2	very low	$2m(=20)$	3	just $\mu_j = [100, 4, 5]$
3	low	$5m(=25)$	5	all of them
4	low	$5m(=25)$	5	all of them
5	very low	19	3	electromagnetic and dielectric

the test locations coincide with the locations of the inclusions; however, for other locations, this number is a very small order of magnitude equal to or less than 0.

In case 5, we have a combination of inclusions. In this case if we consider $\frac{norm(A_{\alpha d})}{norm(A_{\alpha p})}$ ratio, as a criterion of direction, where $A_{\alpha d}$ and $A_{\alpha p}$ are for dielectric and permeable inclusions, respectively, it is equal to 20.65. Therefore, the ratio of $norm(A_{\alpha p})$ to $norm(A_{\alpha d})$ acts similarly to SNR, and thus

permeable inclusion cannot be restored. Therefore for $\varepsilon = [4, 1, 3, 5i, 1]\varepsilon_0$ and $\mu = [1, 1.1, 3, 3+2i, 5i]\mu_0$, the second and last inclusions are not restored.

By increasing the frequency to 29 GHz, the overall locating performance is improved.

8. CONCLUSION

In this paper, a new formulation for scattering matrix using MUSIC algorithm is presented to locate dielectric, permeable, electromagnetic, lossy inclusions and combination of them in a noise-free and a noisy biaxial anisotropic background. In this work, the locations of 5 isotropic ellipsoid inclusions in a permeable anisotropic background are found. This issue is studied for five cases such as dielectric, permeable, electromagnetic, lossy electromagnetic inclusions, and combination of them. Different inclusions with small, big, and middle values of ε_j and μ_j are also investigated. In all the cases, in a noise-free background the results are good. The cases with a noisy background are investigated. The number of singular values of signal subspace of A_α for SNR = 5 dB is less than noise-free background. Also, in a noise-free background all dielectric inclusions with big or small values of ε_j simultaneously, but in a noisy background, the inclusions with higher values of ε_j, which is closer to real background, are restored.

At the end, the proposed formulation for the extended targets is investigated, and the simulation results show that this formulation is appropriate for extended targets.

Therefore, the new proposed formulation of an anisotropic permeable background for object locating predicts the locations very well in a noise-free background and almost well in a noisy background for point-like inclusions or extended. As frequency increases from 1 to 29 GHz, the results have become better.

REFERENCES

1. Nikolova, N. K, "Microwave imaging for breast cancer," *IEEE Microwave Magazine*, Vol. 12, No. 7, 78–94, 2011.
2. Semnani, A., I. T. Rekanos, M. Kamyab, and M. Moghaddam, "Solving inverse scattering problems based on truncated cosine Fourier and cubic B-spline expansions," *IEEE Transactions on Antennas and Propagation*, Vol. 60, No. 12, 5914–5923, 2012.
3. Shamsaddini, M., A. Tavakoli, and P. Dehkhoda, "Inverse electromagnetic scattering of a dielectric cylinder buried below a slightly rough surface using a new intelligence approach," *23rd Iranian Conference on Electrical Engineering (ICEE)*, 391–396, 2015.
4. Cheney, M., "The linear sampling method and the MUSIC algorithm," *Inverse Problems*, Vol. 17, No. 4, 591–595, 2001.
5. Bao, G., J. Lin, and Sé. M. Mefire, "Numerical reconstruction of electromagnetic inclusions in three dimensions," *SIAM Journal on Imaging Sciences*, Vol. 7, No. 1, 558–577, 2014.
6. Chen, X. and K. Agarwal, "MUSIC algorithm for two-dimensional inverse problems with special characteristics of cylinders," *IEEE Transactions on Antennas and Propagation*, Vol. 56, No. 6, 1808–1812, 2008.
7. Agarwal, K. and X. Chen, "Applicability of MUSIC-type imaging in two-dimensional electromagnetic inverse problems," *IEEE Transactions on Antennas and Propagation*, Vol. 56, No. 10, 3217–3223, 2008.
8. Joh, Y. D. and W. K. Park, "Structural behavior of the MUSIC-type algorithm for imaging perfectly conducting cracks," *Progress In Electromagnetics Research*, Vol. 138, 211–226, 2013.
9. Joh, Y. D., Y. M. Kwon, and W. K. Park, "MUSIC-type imaging of perfectly conducting cracks in limited-view inverse scattering problems," *Applied Mathematics and Computation*, Vol. 240, 273–280, 2014.
10. Park, W. K., "Properties of MUSIC-type algorithm for imaging of thin dielectric inhomogeneity in limited-view inverse scattering problem," *Progress In Electromagnetics Research M*, Vol. 37, 109–118, 2014.

11. Ahn, C. Y., K. Jeon, and W. K. Park, "Analysis of MUSIC-type imaging functional for single, thin electromagnetic inhomogeneity in limited-view inverse scattering problem," *Journal of Computational Physics*, Vol. 291, 198–217, 2015.
12. Ciuonzo, D., G. Romano, and R. Solimene, "Performance analysis of time-reversal MUSIC," *IEEE Transactions on Signal Processing*, Vol. 63, No. 10, 2650–2662, 2015.
13. Devaney, A. J., "Time reversal imaging of obscured targets from multistatic data," *IEEE Transactions on Antennas and Propagation*, Vol. 53, No. 5, 1600–1610, 2005.
14. Gruber, F. K., E. A. Marengo, and A. J. Devaney, "Time-reversal imaging with multiple signal classification considering multiple scattering between the targets," *The Journal of the Acoustical Society of America*, Vol. 115, No. 6, 3042–3047, 2004.
15. Marengo, E. A., F. K. Gruber, and F. Simonetti, "Time-reversal MUSIC imaging of extended targets," *IEEE Transactions on Image Processing*, Vol. 16, No. 8, 1967–1984, 2007.
16. Ammari, H., E. Iakovleva, and D. Lesselier, "Two numerical methods for recovering small inclusions from the scattering amplitude at a fixed frequency," *SIAM Journal on Scientific Computing*, Vol. 27, No. 1, 130–158, 2005.
17. Ammari, H., E. Iakovleva, D. Lesselier, and G. Perrusson, "MUSIC-type electromagnetic imaging of a collection of small three-dimensional inclusions," *SIAM Journal on Scientific Computing*, Vol. 29, No. 2, 674–709, 2007.
18. Rodeghiero, G., M. Lambert, D. Lesselier, and P. P. Ding, "Electromagnetic MUSIC imaging and 3-D retrieval of defects in anisotropic, multi-layered composite materials," *The 9th International Conference on Computational Physics (ICCP9)*, A05–05, 2015.
19. Shirmehenji, F., A. Zeidaabadi Nezhad, and Z. H. Firouzeh, "Object locating in anisotropic dielectric background using MUSIC algorithm," *2016 8th International Symposium on Telecommunications (IST)*, 396–400, 2016.
20. Chen, L. F., C. K. Ong, C. P. Neo, V. V. Varadan, and V. K. Varadan, *Microwave Electronics: Measurement and Materials Characterization*, John Wiley & Sons, 2004.
21. Liu, L., L. B. Kong, G. Q. Lin, S. Matitsine, and C. R. Deng, "Microwave permeability of ferromagnetic microwires composites/metamaterials and potential applications," *IEEE Transactions on Magnetics*, Vol. 44, No. 11, 3119–3122, 2008.
22. Pozar, D. M., *Microwave Engineering*, John Wiley & Sons, 2009.
23. Collin, R. E., *Foundations for Microwave Engineering*, John Wiley & Sons, 2007.
24. Herczyński, A., "Bound charges and currents," *American Journal of Physics*, Vol. 81, No. 3, 202–205, 2013.
25. Ammari, H. and H. Kang, *Polarization and Moment Tensors: With Applications to Inverse Problems and Effective Medium Theory*, Vol. 162, 2007.
26. Catapano, I., L. Di Donato, L. Crocco, O. M. Bucci, A. F. Morabito, T. Isernia, and R. Massa, "On quantitative microwave tomography of female breast," *Progress In Electromagnetics Research*, Vol. 97, 75–93, 2009.
27. Ball, J. E., " Low signal-to-noise ratio radar target detection using linear support vector machines (L-SVM)," *2014 IEEE Radar Conference*, 1291–1294, 2014.
28. Chevalier, P., A. Ferrol, and L. Albera, "High-resolution direction finding from higher order statistics: The 2rmq-MUSIC algorithm," *IEEE Transactions on Signal Processing*, Vol. 54, No. 8, 2986–2997, 2006.
29. Dobrzański, L. A., M. Drak, and B. Zibowicz, "Materials with specific magnetic properties," *Journal of Achievements in Materials and Manufacturing Engineering*, Vol. 17, No. 1–2, 37–40, 2006.